ORIGINAL PAPER

Landslide-tunnel interaction mechanism and numerical simulation during tunnel construction: a case from expressway in Northwest Yunnan Province, China

Jiawei Fan[1] · Yufang Zhang[2] · Wenjiao Zhou[2] · Chuan Yin[3]

Abstract

The excavation of the tunnel on the expressway in northwest Yunnan province induced landslide and a series problem such as ground surface cracks of the slope, sliding of the slope, and cracks in the tunnel lining. This research aims to reveal the interaction relationship between the tunnel and the landslide from the prospective of field monitoring and numerical simulation. Firstly, the engineering geological conditions of the slope where the tunnel was located were obtained by field investigation. The "landslide traction segment-tunnel longitudinal tensile failure" mode was put forward based on the spatial relationship between the tunnel and the landslide. Secondly, field monitoring methods were adopted to monitor the surface displacement of the slope, the deep-seated displacement of the landslide, and the propagation of cracks in the tunnel lining. Finally, three-dimensional numerical models were established to investigate the stability of the slope and the tunnel under natural conditions, tunnel excavation conditions, and rainfall conditions. The field investigation results, field monitoring results, and numerical simulation results illustrated that: (1) The tunnel traversed the traction segment of the landslide body in parallel, and tensile failure or shear dislocation failure would occur at different stages of the interaction between the tunnel and the landslide. (2) Two sliding layers were discovered in the landslide, the shallow creep sliding layer and the deep creep sliding layer, which corresponded to the tensile failure and shear dislocation failure modes proposed in the "landslide traction segment-tunnel longitudinal tensile failure" mode, respectively. (3) The slope was in an unstable state under natural conditions. The tunnel excavation disrupted the initial stress equilibrium of the slope, resulting in stress release of the surrounding rock mass. Both excavation and rainfall would exacerbate the deformation of the landslide and the tunnel. Eventually, control measures based on the control grouting technology of the steel floral tubes were suggested to counter with landslide-tunnel deformation problems.

Keywords Landslide-tunnel interaction · Landslide · Expressway tunnel · Field monitoring · Numerical simulation

Introduction

Landslide is a typical engineering geological hazard which mostly occurs in mountainous areas (Konagai et al. 2005; Avanzi et al. 2013; Pudasaini and Miller 2013; Poisel et al. 2016; Yan et al. 2019; Li et al. 2020; Wei et al. 2020; Zhu et al. 2020). As a common structure used in expressway construction in mountainous areas, tunnel is inevitably constructed to traverse mountains and hills so as to ensure the smoothness of the expressway (Sun et al. 2010; Holzleitner et al. 2013; Li et al. 2014; Lalagüe et al. 2016; Zhang et al. 2018; Das et al. 2020; Tsao et al. 2021). When tunnel construction encounters ancient landslides, the excavation of the tunnel will react to the ancient landslides, inducing damages to the tunnel structures and causing potential casualties and economic losses (Lari et al. 2014; Zhou et al. 2015; Alonso et al. 2016; Iverson and George 2016; Huang et al. 2017; Wei et al. 2019; Chen et al. 2020b; Wilfing et al. 2021; Zhang et al. 2021). Therefore, it is imperative to deepen the understanding of the landslide-tunnel interaction mechanism.

✉ Yufang Zhang
  2723614088@qq.com

1 China Academy of Railway Sciences, Beijing, China

2 Railway Engineering Research Institute, China Academy of Railway Sciences Co. Ltd, Beijing, China

3 Yunnan Construction and Investment Holding Group Co., Kunming 650000, Yunnan, China

The research on the interaction relationship between landslides and tunnels has been conducted by a series of scholars in the last decade. The method of monitoring by means of inclinometer, Light Detection and Ranging (LiDAR), or Interferometric Synthetic Aperture Radar (InSAR) has been adopted by a huge number of scholars (Walton et al. 2014; Bandini et al. 2015; Chen et al. 2015; Tang et al. 2015; Barla et al. 2016; Fiorucci et al. 2017; Kromer, 2017; Huang et al. 2018; Desrues et al. 2019; Sun et al. 2019; Chen et al. 2020a; Tian et al. 2021). Additionally, the method of numerical simulation has also been utilized widely (Lu et al. 2013; Barla et al. 2015; Li et al. 2015; Wu et al. 2015; Barla et al. 2016; Lu et al. 2018; Gattinoni et al. 2019; Sun et al. 2019; Vassallo et al. 2019; Zhou et al. 2019; Komu et al. 2020; Guo et al. 2021).

Jiao et al. (2013) performed a 12-month long-term monitoring work. They established three-dimensional numerical models using FLAC3D and GEO-SLOPE to investigate the influence of tunnel excavation to an existing ancient landslide, which provided technical guidance to the tunneling project management. Kaya et al. (2016) combined kinematic, limit equilibrium, and numerical stability analysis methods to investigate failure mechanism of a tunnel cut slope and portal slope, indicating that cut slope failure was controlled by low strength parameters of the rock mass, and portal slope failure was controlled by both effects of joints and low strength parameters of the rock mass. Bayer et al. (2017) adopted InSAR and inclinometer to monitor the ground surface displacement and deep-seated displacement of a landslide, claiming that the excavation of the tunnel was the primary reason for the landslides, and rainfall had less influence on the landslides in this case. Kaya et al. (2017) used finite element method to analyze failure mechanism of a tunnel portal during excavation and the effectiveness of corresponding remediation methods, concluding that insufficient initial support and weathering rock masses were the causes of failure, and rock retaining wall with jet grout columns were proved effective as remediation measures. Wang et al. (2020) utilized field investigation, displacement monitoring, and numerical simulation methods to research the interaction between the ancient landslide and the tunnel, contending that both tunnel excavation and rainfall contributed to the development of the landslide. Duan et al. (2021) focused on the impact of rainfall conditions on the stability of the tunnel exit slope. The stability was investigated under different rainfall types and intensities using GeoStudio numerical simulation software, declaring that the rainstorm condition was the most unfavorable case to the tunnel exit slope stability. However, although the interaction between the landslide and the tunnel has been studied to a certain extent, the interaction mechanism has not been thoroughly analyzed.

To thoroughly analyze the interaction mechanism between the landslide and the tunnel, a case from expressway in northwest Yunnan province was investigated in this research. Firstly, a "landslide traction segment-tunnel longitudinal tensile failure" model was proposed based on the mechanical analysis by considering the spatial relationship between the landslide and the tunnel. Additionally, field investigation and long-term monitoring efforts had been continuously conducted during the process of construction. Finally, a series of three-dimensional numerical models were constructed by using FLAC3D to investigate the proposed failure mode further.

Study site

### Slope geomorphology and geotechnical investigations

The area to which the tunnel belongs is a tectonic erosion and denudation area of alpine and valley landforms. The portal slope of the tunnel is located on the north side of the ridge with a strike of 262°. The maximum elevation of the mountain is 3162 m, and the rate of the slope is 31°. The bottom of the slope is a river, at which the elevation is 2422 m. The relative height difference between the top of the mountain and the river's bottom is 740 m. The tunnel traverses the natural slope in parallel.

The tunnel is a left and right separated tunnel locating in Yunnan Province, China. The length of the tunnel is 1260 m. The excavation of the left tunnel began on May 4th, 2016. The excavation of the right tunnel started on October 30th, 2016. However, cracks and dislocations were discovered on the slope of the tunnel portal by the construction unit in 2015. A crack with a spreading direction of 259° with a length of 10 m, a width of 30 cm, and a depth of 40 cm was discovered where the elevation was 160 m directly above the right tunnel. Besides, a crack with a spreading direction of 259° was also discovered where the elevation was 60 m directly above the left tunnel. Additionally, cracks were also discovered on tunnel lining within 40 m of the tunnel portal during the tunnel construction. The detailed layout of cracks on the portal slope and tunnel lining is shown in Fig. 1.

Stratum lithology and geological tectonic features

To discover the groundwater level and strata of the slope, thirteen boreholes were drilled. The layout scheme of boreholes is shown in Fig. 2, and the corresponding geological cross-section diagrams are shown in Fig. 3. As a result, the strata of the slope are overlying Quaternary deposits, mainly composed of gravelly silty clay and gravel soil. The lower strata are composed of Middle Triassic (T_1) Formation strongly moderately weathered gray and gray-brown

Fig. 1 The detailed layout of cracks on the portal slope and tunnel lining

(a)

(b)

(c)

(d)
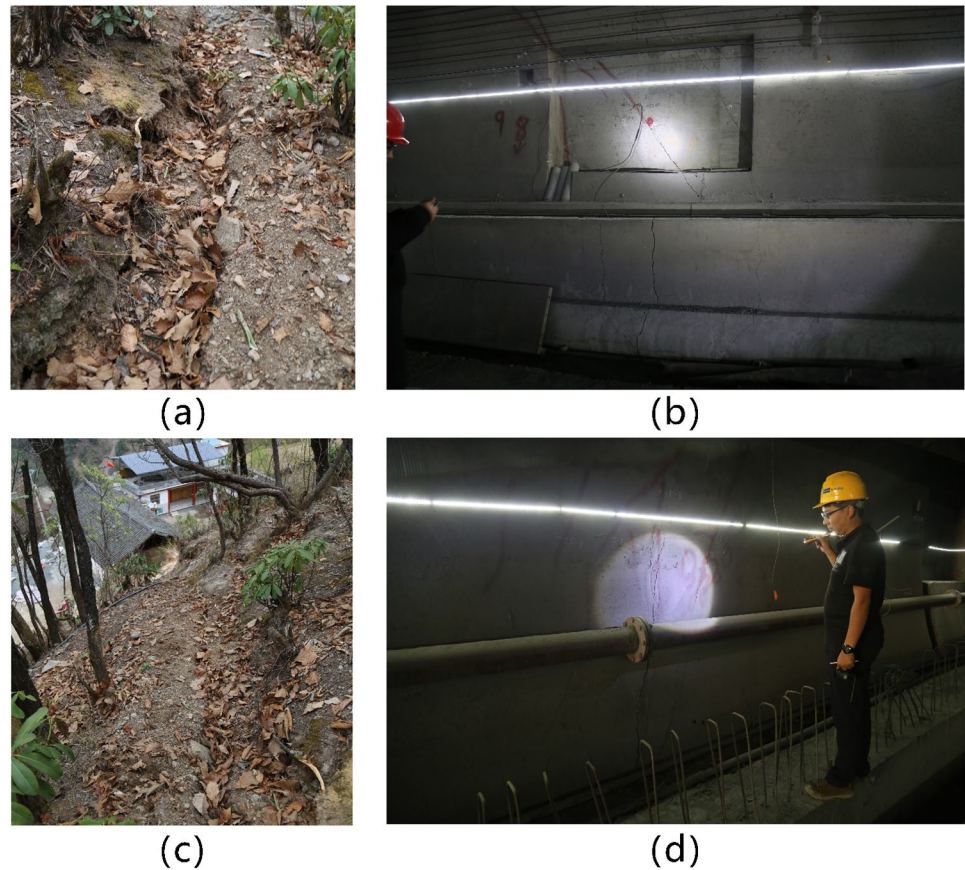
slate, strongly weathered slate, and moderately weathered slate. The detailed information is shown below: (1) gravelly silty clay (Q_4^{dl}), with the appearance of earthy yellow, gray, dark gray, composed of 10~30% of angular crushed stone, and the particle size is from 3 to 5 cm. The allowable bearing capacity is 220 kPa. (2) Gravel soil (Q_4^{dl}), with the appearance of earthy yellow, gray, dark gray, composed of 50% of angular crushed stone, with mixed particle size. The allowable bearing capacity is 300 kPa. (3) Slate (T_1), with the appearance of gray, dark gray, with well-developed joints and fissures. The allowable bearing capacity is 400 kPa.

According to the situation of ground surface exposure and tunnel excavation, the local tectonic activity is severe. As a result, the joints and fissures are developed, and the rock mass is broken. The bedrock occurrence is 98°∠56° on the left bank of the river, with an anti-dip. A set of downwardly inclined structural planes are measured above the tunnel portal, with an occurrence of 315°∠29°. There are two main types of groundwater in the study site, which are pore water in Quaternary accumulation layers and bedrock fissure water. The bedrock fissure water is mainly in the strong weathering zone with developed fissures, and the groundwater level exposed by the drilling during the survey is relatively high.

Theoretical analysis of the landslide-tunnel interaction

When the tunnel traverses through a slope that has the potential of landslide, the deformation of the landslide will cause the deformation of the tunnel. Meanwhile, the excavation of the tunnel may also cause or aggravate the deformation of the landslide. The landslide-tunnel interaction is related to time distribution and spatial distribution. Thus, it is significant to specify the spatial relationship of the tunnel and the landslide at the first place.

Spatial relationship between the tunnel and the landslide

Based on the spatial relationship between the axial of the tunnel and the main sliding direction of the landslide, the spatial relationship between the tunnel and the landslide could be divided into three modes, which are the tunnel traverses the landslide in parallel, orthogonal, and skew forms. The parallel form refers that the main sliding direction of the landslide is parallel or approximately parallel (0~20°) to the tunnel axis. The orthogonal form refers that the main sliding direction of the landslide is perpendicular or approximately perpendicular (70~90°) to the tunnel
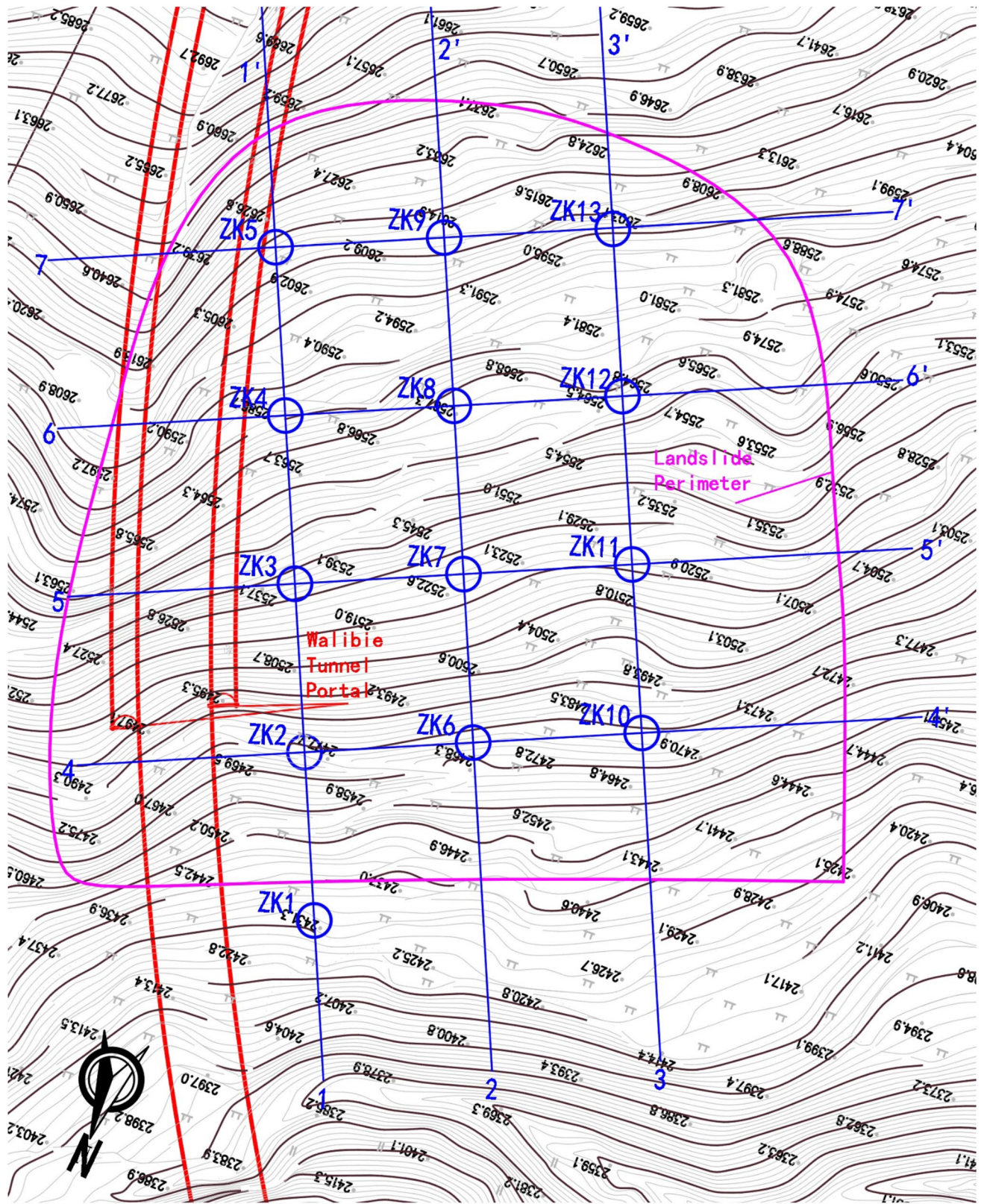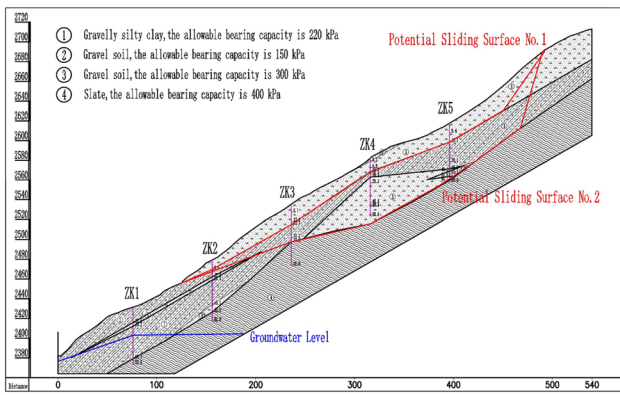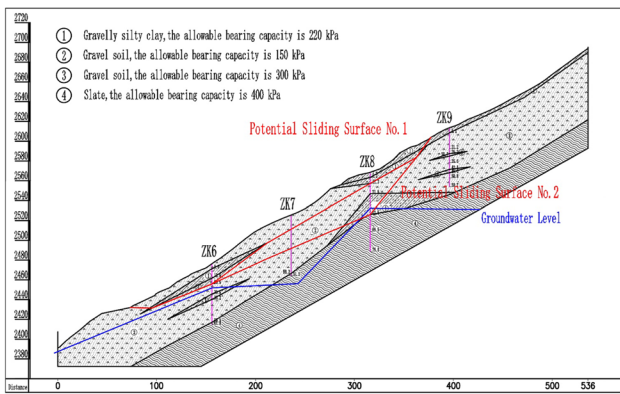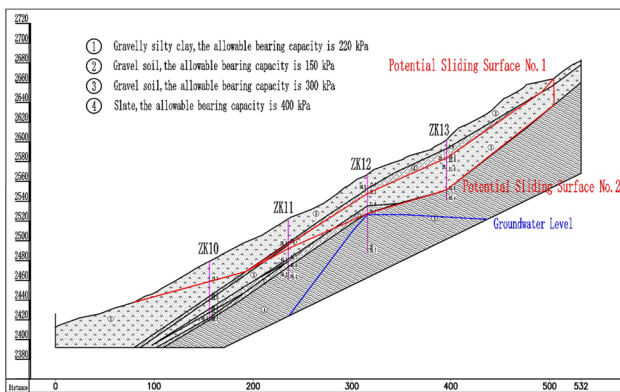
Fig. 2 The layout scheme of boreholes

a) 1-1' cross section diagrams

b) 2-2' cross section diagrams

c) 3-3' cross section diagrams

Fig. 3 Geological cross section diagrams

axis. The skew form refers that the angle between the main sliding direction of the landslide and the axial direction of the tunnel is between 20° and 70°.

The segments of the landslide could be divided into traction segment, sliding segment, and anti-sliding segment from the view of the longitudinal section of the landslide (Mandal and Mondal 2019). The traction segment is located in the middle and upper parts of the landslide. The failure of the traction segment is due to the loss of support from

the lower part, and tensile cracks would occur at the trailing edge. The sliding segment is mainly manifested as the overall translation movement during the process of the landslide deformation. The anti-sliding segment is mainly the compression area in the stress state of the landslide. Tunnels traversing through different positions in the landslide body are subjected to different effects such as stretching, shearing, or squeezing transmitted from the landslide body, which cause different deformation characteristics of the tunnel. In this case study, the decline of the tunnel is 332°, and the decline of the main direction of the landslide is 330°. The tunnel traverses the landslide in parallel from the position of the landside traction segment.

"Landslide traction segment-tunnel longitudinal tensile failure" mode

As shown in Fig. 4, the "landslide traction segment-tunnel longitudinal tensile failure" mode is in the situation that the tunnel traverses the traction segment of the landslide body in parallel. This failure mode mainly occurs in the creeping stage of the main sliding zone of the landslide. The strength of the main sliding zone is less than the exerted stress, which generates downward and forward creeping deformation, forcing the sliding body of the sliding section to compress, inducing the traction segment to creep downward and forward. At this moment, ring-shaped, steep but discontinuous tensile cracks are formed on the ground at the rear edge of the landslide. These cracks enlarge gradually, causing the tunnel traversing through the traction segment to generate tensile deformation. As the stability of the landslide body declines, when the landslide body is in the compression stage, which means the anti-sliding segment is obviously compressed by the sliding segment, it causes the traction segment to deform gradually. With the time going on, if the back wall of the landslide is hard rocks, the tunnel is subjected to shear dislocation failure. If the back wall of the landslide is soft rocks, the tunnel is bent and damaged. The development of this "landslide traction segment-tunnel longitudinal tensile failure" mode is generally divided into four stages.

(1) The landslide body is in a long-term stable state under natural conditions, and no obvious cracks opening and dislocation are discovered on the ground surface.

(2) Under the excavation of the tunnel, when the landslide body is in the creeping stage, the surface cracks on the trailing edge of the landslide body are slightly enlarged due to the influence of the tunnel excavation, as shown in Fig. 5a. During the opening of the trailing edge, the full section of the tunnel is deformed and destroyed in tension, and obvious tensile cracks are generated in the tunnel (Zhang 2009). Since the sliding surface is not penetrated, there are no signs of dislocation.

Fig. 4 The diagram of the "landslide traction segment-tunnel longitudinal tensile failure" mode
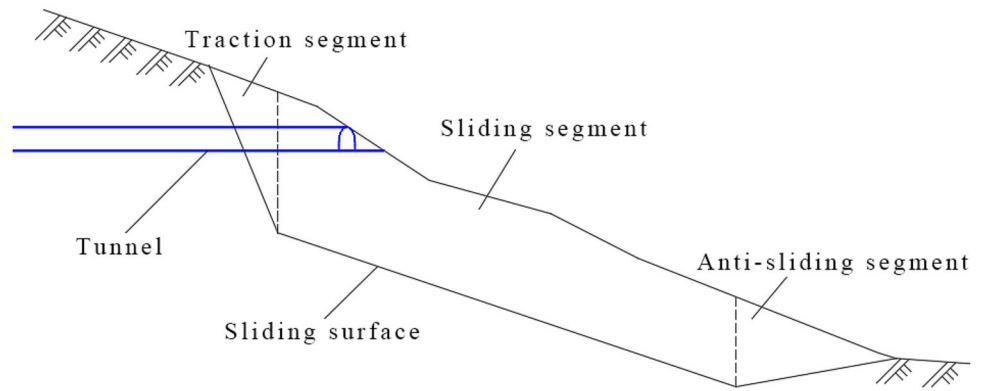
(3) With the continuous excavation of the tunnel, when the landslide body is in the compression stage, as shown in Fig. 5b, the sliding surface gradually penetrates so that the tunnel has a significant downward movement along the sliding surface, causing the tunnel to be damaged (Zhang 2009). If the sliding body is soft rocks, the tunnel is bent and damaged. If the sliding body is hard rocks, the tunnel is dislocated and destroyed.

(4) When the landslide body slides, the tunnel moves simultaneously with the landslide body. The tunnel is completely dislocated at the sliding surface.

In situ monitoring and deformation analysis

Ground surface displacement monitoring

The ground surface displacement monitoring had been continuously conducted from March to November in 2017. As shown in Fig. 6, eighteen surface displacement observation points have been installed on the upward slope of the tunnel portal. Figure 7 indicated that the displacements of X, Y, and Z directions (the positive directions of X, Y, and Z are Northward, Westward, vertically upward, respectively) increased with the time going

on, and the increase rate of the displacement was approximately linearly at a uniform speed. Among them, the displacement in the X direction increased toward the north direction, and the largest displacement was observation point No. 10 with about 62 mm. The displacement in the Y direction increased toward the east direction, and the largest displacement was the observation point No. 13 with about 24 mm. The displacement in the Z direction is settlement deformations. The largest settlements were observation points No. 9 and No. 15, reaching 24 mm.

By calculating the displacement directions of these 18 monitoring points, the displacement direction was between NW1° and NW10°. The average displacement direction was NW6°. The maximum displacement direction point was No. 13, and its displacement direction was toward the north direction. The angle between the axial direction of the tunnel portal (NW28°) and the maximum displacement direction was 28°.

Deep-seated displacement monitoring

To investigate the deformation characteristics of the landslide, two displacement monitoring holes of 62 m deep were drilled on the centerline at the portal of the left and right tunnels. The monitoring holes were located above the tunnel and below the slopes. Figure 8 indicated that the SZ-1 hole above the tunnel portal observed a large displacement in the range of 32~36 m, and the SZ-2 hole located under

Fig. 5 Stress diagram of the "landslide traction segment-tunnel longitudinal tensile failure" mode in different stages

a) Stress diagram of the tunnel in creep stage   b) Stress diagram of the tunnel in extrusion stage
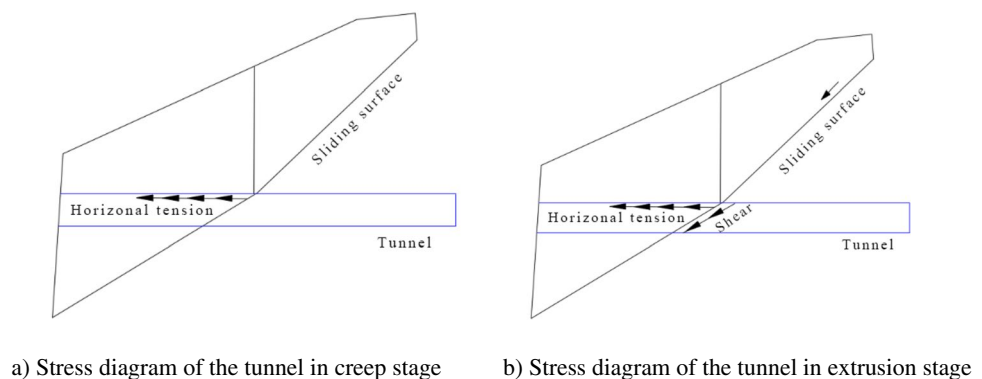
Fig. 6 Layout of observation points
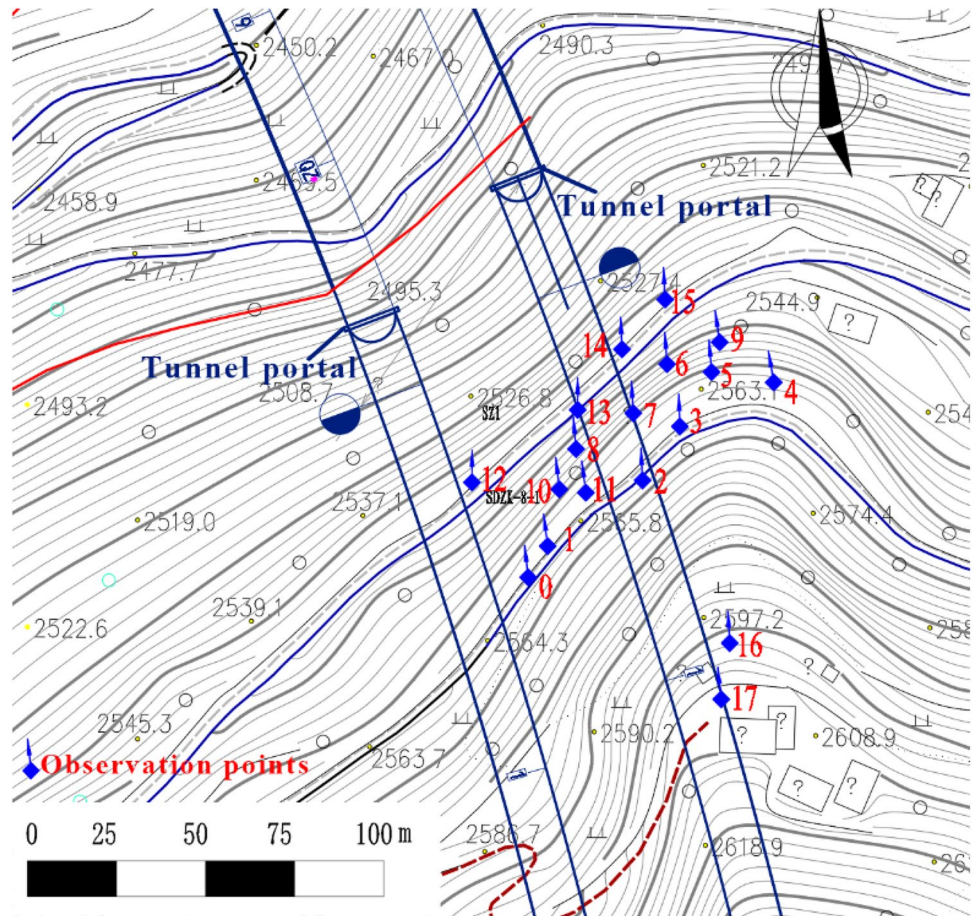
the retaining wall of the construction platform of the tunnel portal observed a large deformation in the range of 44~48 m.

Tunnel crack monitoring

The JMZX-212HAT surface-mount concrete strain gauge (with temperature compensation function) with a strain measurement accuracy of 0.5% FS (2 μɛ) and a strain resolution of 0.25% FS (1 μɛ) was used to monitor the propagation of cracks on the lining of the left and right tunnels. This type of strain gauge has the characteristics of high sensitivity, high precision, and high stability. Through the comprehensive tester, the strain of the tunnel lining concrete can be measured so as to obtain the development of the cracks and the stress state of the lining.

Eleven typical cracks on the lining of the tunnel were selected for monitoring, including 6 on the left tunnel and 5 on the right tunnel. The test results of 11 typical crack widths are shown in Table 1.

Analysis of the monitoring data

Combined with the information of the ground surface displacement distribution, the deep-seated displacement monitoring

curve, and the tunnel crack distribution, the results suggested that there were different degrees of deformation in the tunnel and the landslide body from the position of the cracks above the tunnel portal to the slope range of the SZ-2 monitoring hole at the lower part of the abutment. Based on the positions of these deformations, it can be inferred that two creep sliding layers existed in the range of the landslide body, which were the shallow creep sliding layer and the deep creep sliding layer.

Firstly, the analysis was focused on the shallow creep sliding layer. A crack with a spreading direction of 259° was observed on the ground surface 60 m above the left tunnel portal, which was shown in Fig. 1c. The corresponding tunnel mileage of the crack was ZK+020. Meanwhile, cracks were also discovered on the left and right sides walls of the tunnel in the mileage range of ZK+010~020, which was shown in Fig. 1d. The crack width was about 1 mm, and the crack dip angle was between 36° and 41°. Additionally, the SZ-1 deep-seated displacement monitoring hole located above the tunnel portal also observed a large displacement in the range of 32~36 m. Combining the above deformation characteristics, it was speculated that the depth of the shallow creep sliding layer was about 32 m. Since cracks observed in the mileage range of ZK+010~020 were not fully developed, and no annular cracks and dislocations were
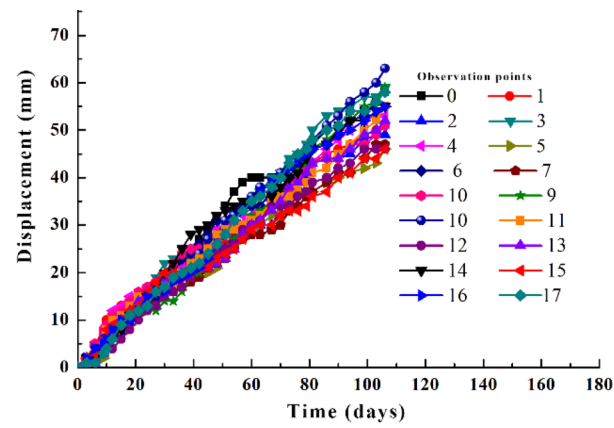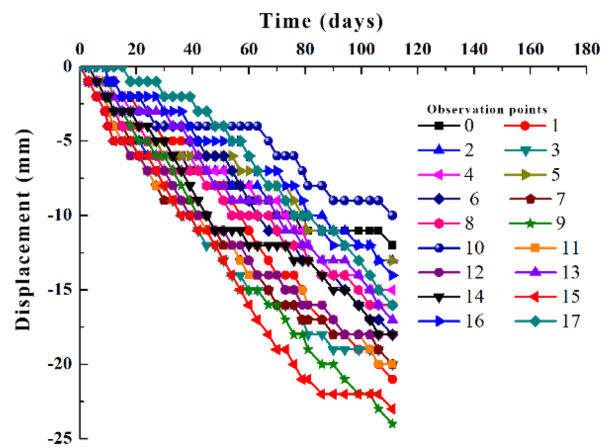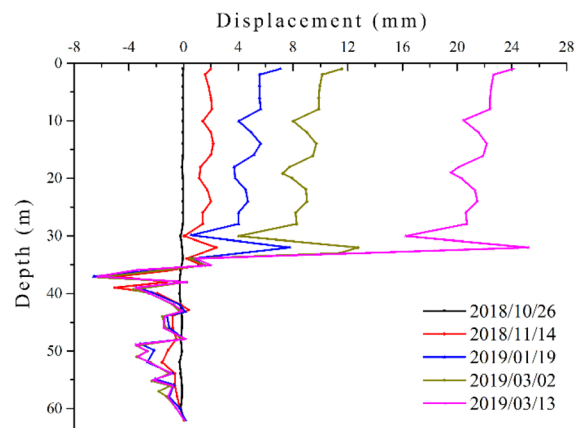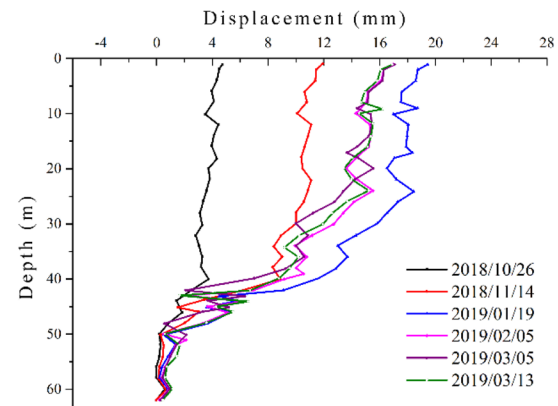
a) X direction
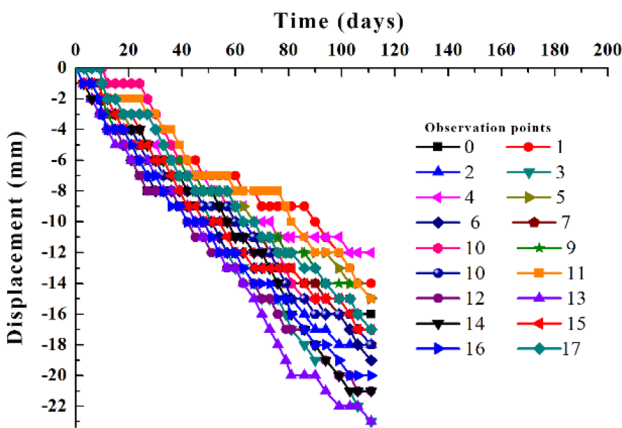
b) Y direction

c) Z direction

Fig. 7 Observation results of the ground surface displacements

a) Displacement along the slope of SZ-1 monitoring hole

b) Displacement along the slope of SZ-2 monitoring hole

Fig. 8 Displacement along the slope of SZ-1 and SZ-2 monitoring hole

formed, the shear stress of the shallow creep sliding layer was not large enough to cause the shar failure of the tunnel. Thus, the primary form of failure of the tunnel was tension, which conformed to the failure mode, as shown in Fig. 3a.

Secondly, the analysis was focused on the deep creep sliding layer. A crack with a spreading direction of 259° was observed on the ground surface 160 m above the right tunnel portal, which was shown in Fig. 1a. The corresponding tunnel mileage of the crack was YK+030. A huge number of fully developed cracks were discovered on the tunnel's left and right sides walls in the mileage range of YK+025~034, which was shown in Fig. 1b. The widest crack width was about 15 mm. The crack dip angle was between 36° and 41°. A dislocation of about 1~2 mm was observed at the mileage location of YK+025, and obvious penetrated cracks were discovered at the vault position of YK+034. Additionally, the SZ-2 deep-seated displacement monitoring hole under the retaining wall of the construction platform also observed a large displacement in the range of 44~48 m. Combining the above deformation characteristics, it was speculated that the depth of the deep creep sliding layer was about 44 m. Since cracks observed in the mileage range of YK+025~034 were completely developed, and annular cracks and dislocations were completely formed, it indicated that the tunnel was sheared and destroyed in dislocation, which conformed to the failure mode as shown in Fig. 3b.

Table 1 Test results of 11 typical crack widths on the lining of tunnel

Monitoring series number	Monitoring location	Initial crack width (mm)	Final crack width (mm)	Average rate of change (mm/d)
WJZ-01	ZK+020 right side	5.07	5.765	0.0015
WJZ-02	ZK+038 right side	0.72	1.058	0.0007
WJZ-03	ZK+040 right side	0.36	0.346	-0.00003
WJZ-04	ZK+037 left side	1.93	2.135	0.0004
WJZ-05	ZK+030 right side	1.99	2.174	0.0004
WJZ-06	ZK+015 right side	2.66	2.679	0.00004
WJY-01	YK+033 right side	2.90	2.967	0.0001
WJY-02	YK+026 right side	5.22	6.089	0.0019
WJY-03	YK+030 left side	4.22	4.459	0.0005
WJY-04	YK+024 left side	3.95	4.148	0.0004
WJY-05	YK+027 left side	3.89	3.939	0.0001

From the crack distributions on the rear edge of the ground surface of the landslide and on the lining of the tunnel, the deformation range of the landslide body was roughly the same as that of the tunnel in terms of spatial distribution. In terms of time distribution, although the landslide body had undergone a certain degree of deformation before the tunnel excavation, the deformation of the landslide body continued to increase during the tunnel excavation, and various degrees of cracks, slippage, and collapse occurred in the tunnel excavation area. The excavation of the tunnel caused the groundwater to continuously infiltrate along the cracks of the weathered slate in the direction of the tunnel and soften the sliding surface. As a result, the landslide body deformed and crept along the sliding surface, inducing the tunnel to generate longitudinal cracks and gradually to shear and displace downwards. Obvious dislocation occurred at the mileage of YK+025. These signs indicated that the tunnel excavation aggravated the deformation of the landslide body, and the deformation of the landslide body also caused the deformation of the tunnel. Therefore, from the time and spatial distribution, the deformation of the tunnel was consistent with the deformation of the landslide.

Three-dimensional numerical simulation and slope stability analysis

To further investigate the mechanism of "landslide traction segment-tunnel longitudinal tensile failure" mode, the following numerical simulation method was used to conduct an in-depth exploration under natural condition, excavation condition, and rainfall condition.

Model setup

A model is constructed through finite element numerical simulation software. The specific calculation range, boundary conditions, and element types, and constitutive relation are as follows:

(1) Calculation range: The longitudinal and lateral lengths of the model are 586 m and 450 m, respectively. The vertical length is 310 m, from the bottom of the tunnel to the downward direction. The X direction is perpendicular to the tunnel axis, and the right direction is positive. The Y direction is parallel to the tunnel axis, and the large mileage direction (inward the tunnel) is positive. The Z direction is vertical, and the upward direction is positive.

(2) Boundary conditions: The boundary conditions of the model are set to not allow normal displacement on the side. Therefore, the movable support boundary conditions are used. The bottom surface restricts the displacement in three directions, and the fixed support boundary conditions are used.

(3) Unit type and constitutive relationship: The model is constructed with tetrahedral elements composed of the upper weathered rock layer and the lower bedrock simulated by ideal elastoplastic materials, which conforms to the Mohr-Coulomb yield criterion. The supporting structure of the tunnel is adopted by using 0.5 m thick concrete lining simulated by linear elastic materials.

After grid division, the calculation model contains 267,649 units and 47,456 nodes in total. The gridded models are shown in Fig. 9.

Calculation parameter determination

To determine rock strength parameters, since it was not feasible to acquire undisturbed rock mass samples to conduct indoor tests, in situ dynamic cone penetration tests were carried out during the process of boreholes drilling. Rock strength parameters were determined by empirical relationships. Tensile strength of rocks was determined as zero on the consideration of conservation. Rock densities were determined by physical tests. Parameters of rock layer were

shown in Table 2. In addition, the parameters of the tunnel lining concrete are also determined by previous physical and mechanical test data. The thickness of the tunnel lining concrete is 50 cm. The shear modulus is 20.9 GPa. The bulk modulus is 13.9 Gpa. The density is 2500 kg/m^3.

Simulation results and analysis

Natural condition

The failure of the slope tends to occur along the part with the largest shear strain. Through the increment of the shear strain, the weakest position in the slope can be found out. As shown in Fig. 10, the shear strain increment becomes larger near the vicinity of the planned excavation of the tunnel, which means the sliding potential becomes larger along this high shear strain increment area. The depth of it is about 40 m. The depth of which is consistent with the depth of sliding surface that monitored in situ. The high shear strain increment has a tendency to penetrate upwards. In addition, the shear strain increment value at the slope toe is higher than in other places. Thus, the landslide is in an unstable state before the excavation under natural conditions, which also conforms to the conclusion drawn from field investigation.
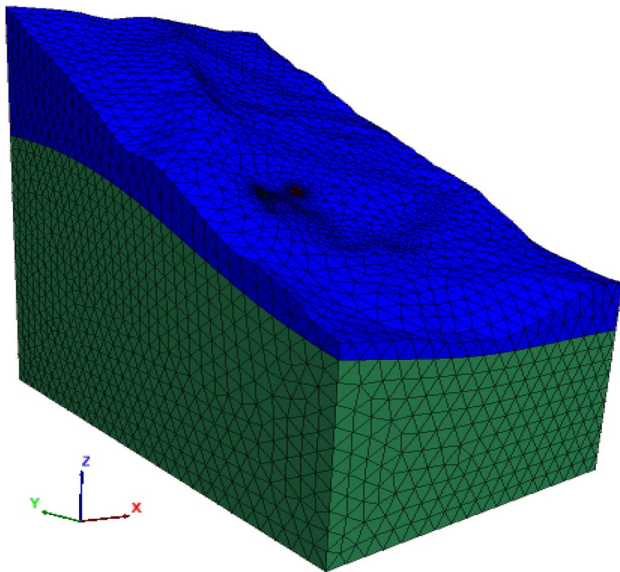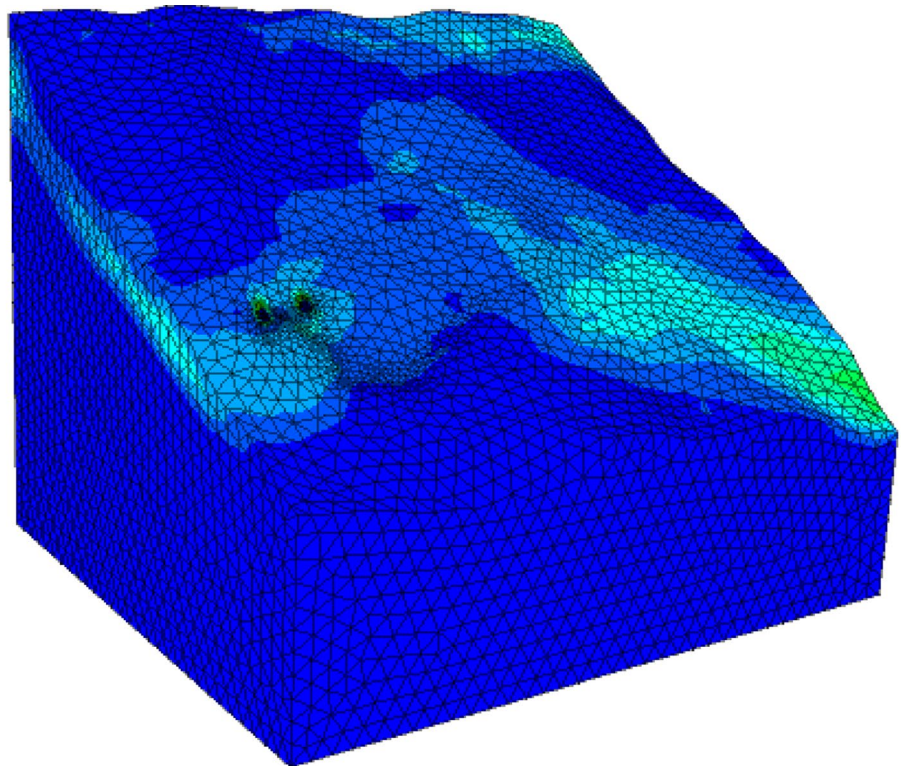

Fig. 9 Gridded model diagram

Excavation condition

Figure 11 shows the maximum shear strain increment sectional diagram of the right tunnel after the excavation. The shear strain increment value at the position of the deep sliding surface of the landslide that the tunnel traverses is much larger. According to the field investigation, the sliding surface is a weak interlayer with soft rock quality, severe weathering, and well-developed joints and fissures. Under the influence of excavation, groundwater converges in the direction of the tunnel cavity, softening the weak interlayer, reducing the strength of the weak interlayer, increasing the shear strain increment. Thus, the stability of the tunnel and the slope has further decreased with the excavation of the tunnel.

After the excavation of the tunnel, large displacements in the three directions of the slope were observed. This is due to the stress release of the tunnel surrounding rock mass caused by the tunnel excavation, which disturbs the equilibrium state of the initial slope, causing the surrounding rock mass to creep and move in the direction of the tunnel circumference.

The displacement of the slope in the X direction after the excavation is shown in Fig. 12a. The landslide body mainly generates displacement to the tunnel, and the value of displacement is small. The maximum displacement occurs 100 m below the tunnel, the value of which is about 2.50 cm. The X-direction displacement near the vicinity of tunnel excavation is about 1 cm. The overall displacement is not large from the X-direction displacement, and the deformation is mainly concentrated within 40 m of the tunnel portal. Compared with cracks observed on tunnel lining, the position of cracks is distributed from ZK(YK)+000 to ZK(YK)+040, which is shown in Table 1. It turns out that the results from numerical simulation are consistent with onsite observations. The displacement of the slope in the Y direction after the excavation is shown in Fig. 12b. The displacements toward the riverside are relatively large at the locations of 90 m and 160 m above the tunnel. The displacement at the location of 90 m above the tunnel on the slope surface is larger, reaching 2.22 cm which is aligned with the ground surface displacement monitoring results in the y direction. The displacement of the slope in the Z direction after the excavation is shown in Fig. 12c. The Z direction is dominated by settlement deformation. The settlement near the tunnel portal is not obvious, the value of which is between 1 and 2 cm, which is roughly aligned with the actual situation on the site. The settlement mainly occurs at 160 m above the tunnel portal, where a settlement of about 8.73 cm occurs,

Table 2 Parameters of rock layer of the slope	Parameters	Bulk modulus	Shear modulus	Cohesion	Friction angel	Tensile strength	Density
	Rock layer	K (GPa)	G (GPa)	c (kPa)	φ (°)	T (kPa)	(kg/m^3)
	Weathered rock	2.5	0.536	100	20	0	2000
	Bedrock	3.7	1.52	500	30	0	2300

Fig. 10 Cloud diagram of maximum shear strain increment under natural conditions

a) 3D view of cloud diagram of maximum shear strain increment under natural conditions)
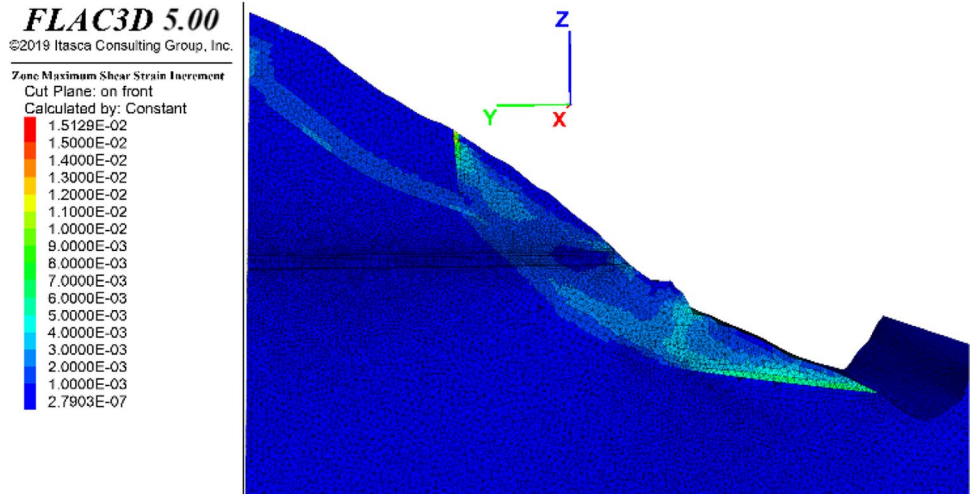
b) Sectional cloud diagram of maximum shear strain increment of the slope before excavation

which is also consistent with the crack depicted in Fig. 1a. The settlement gradually decreases along the slope downward. The position of the maximum settlement is the position of cracks on the rear edge of the landslide, which is also aligned with the actual tunnel excavation process.

In general, the excavation of the tunnel in the landslide section of the slope caused a certain deformation of the slope. Among them, the displacement in the Z direction is relatively large, and the displacements in the X and Y directions are relatively small. This is mainly due to the shallow buried section of the tunnel portal. In addition, the excavation causes the sudden unloading of the surrounding rock, which triggers the upper rock mass of the surrounding rock to deform and move toward the cavern, which promotes the settlement of the rock mass, resulting in certain deformation and settlement of the ground surface. Affected by the

Fig. 11 Sectional cloud diagram of maximum shear strain increment of the slope after excavation
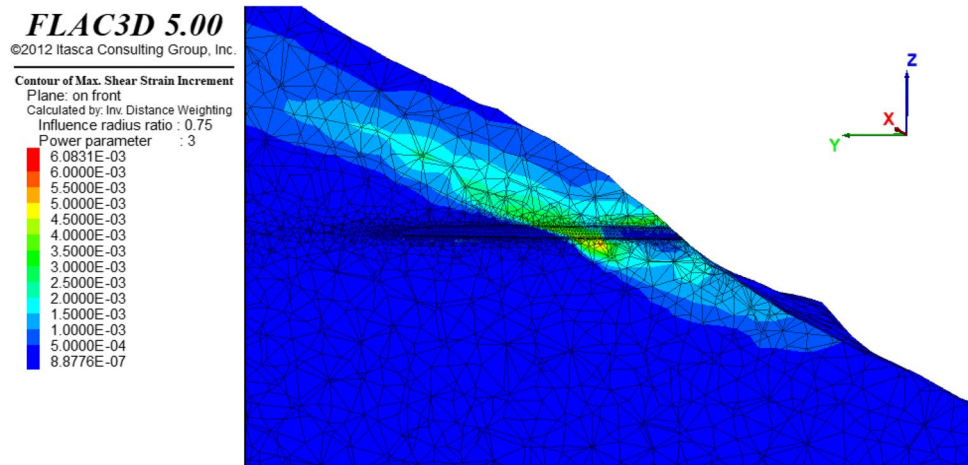
tunnel excavation, the landslide body generates certain creep deformation along the sliding surface, further triggering the tunnel to generate deformation and displacement.

Rainfall condition

Rainfall is one of the major factors that induce the deformation and disaster of the landslide. Strong rainfall in a short period can induce slope diseases and even adversely affect the tunnel. The effect of rainfall obviously weakens the stability of the slope, thereby inducing landslides. By conducting a series of dynamic cone penetration tests during rainfall seasons, it was concluded that strength parameters values tended to reduce 10% compared with non-rainfall season. Therefore, in this numerical simulation, strength parameters values are reduced to 90% of the initial values and the saturated unit weight is considered to simulate the rainfall condition after the tunnel excavation.

Figure 13 shows the maximum shear strain increment sectional diagram of the right tunnel under the rainfall condition after the excavation. The shear strain increment of the landslide body continues to increase under rainfall condition. From the shear strain increment distribution characteristics of the slope, it indicates that the shear strain increment distribution at the front edge of the landslide body gradually extends to the toe of the slope, showing signs of shear slippage.

Under the effect of rainfall, rainwater seepage increases the weight of the slope and reduces the shear strength of the slope body, which further increases the displacement of the slope. As shown in Fig. 14, the distribution characteristics of displacements in the X, Y, and Z directions are not much different from those during tunnel excavation, but the amount of displacement is further increased, and the maximum displacements in the X, Y, and Z directions are increased by 6 cm, 8 cm, and 41 cm, respectively. These maximum displacement positions are all located on the ground surface

near the tunnel portal. The displacements are much larger than those none rainfall conditions, indicating that the slope undergoes a significant deformation under the influence of rainfall, especially for the displacement near the tunnel portal. The effect of rainfall increases the weight of the soil in the shallow surface of the slope, which increases the sliding force of the landslide, and further enhances the deformation of the tunnel.

Discussions

This paper has presented a theoretical and experimental study to investigate the interaction mechanism between the tunnel and the landslide. To sum up, by analyzing the distribution of stratum structure, ground surface deformation characteristics, deep-seated displacement characteristics, and the spatial relationship between the tunnel and the landslide, it indicated that the tunnel was in an unstable state before the tunnel excavation. Affected by the tunnel excavation and rainfall, the stability of the slope further decreased, causing the cracks on the ground surface to spread and the slope body to creep, which induced the tunnel traversed through to generate tensile and shar failure. To better investigate the slope stability changes under natural condition, tunnel excavation condition, and rainfall condition, a series of numerical simulation models have been established to conduct an in-depth analysis.

Comparing the numerical simulation results with in situ monitoring results and field investigation results, it turns out that they are in high consistency. First, the depth of maximum shear strain increment under natural condition is about 40 m, which is consistent with the actual depth of sliding surface from deep-seated displacement monitoring results. Second, when it comes to X-direction displacement of tunnel excavation simulation, the deformation is mainly concentrated within 40 m of the tunnel portal, which is aligned
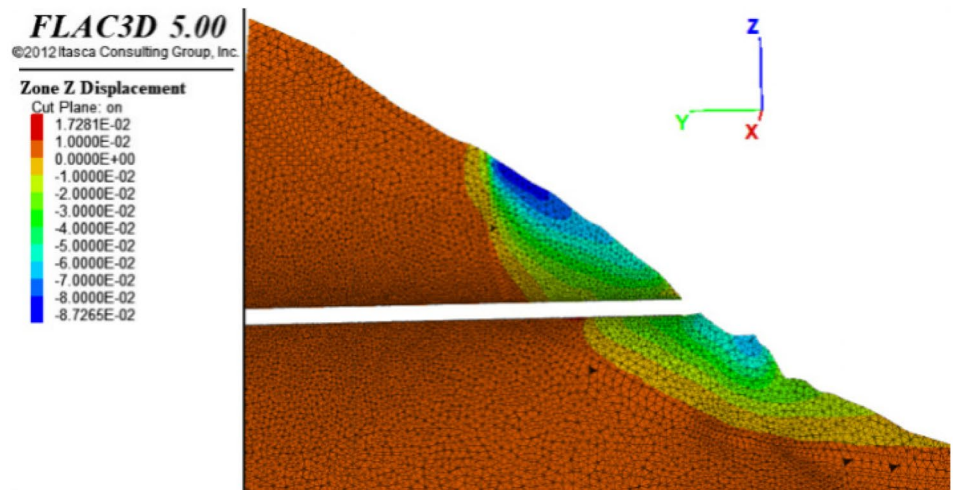
Fig. 12 Displacement cloud diagram of slope in the X, Y, and Z directions after excavation
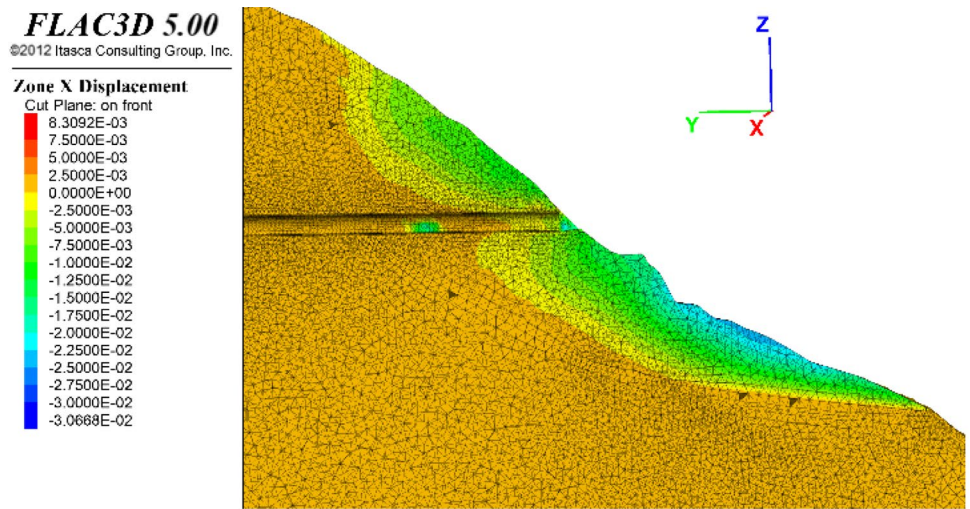
a) Displacement cloud diagram of slope in X direction after excavation
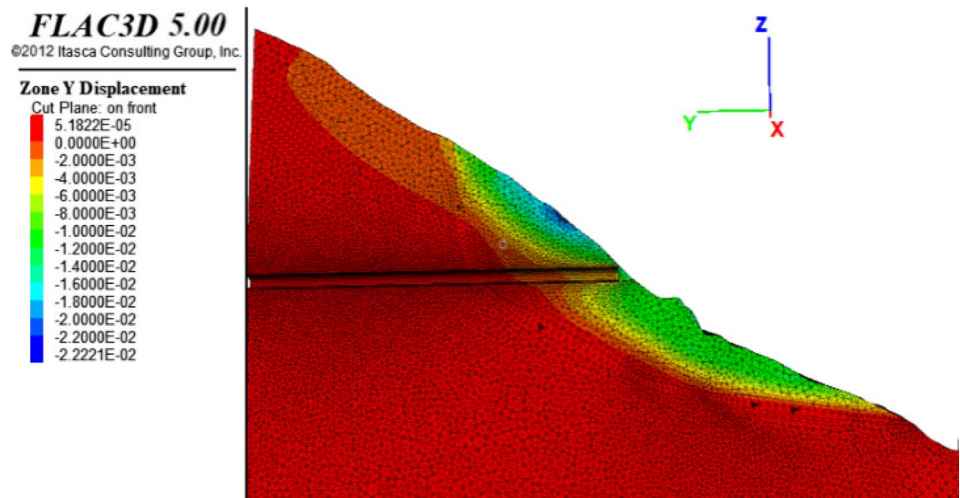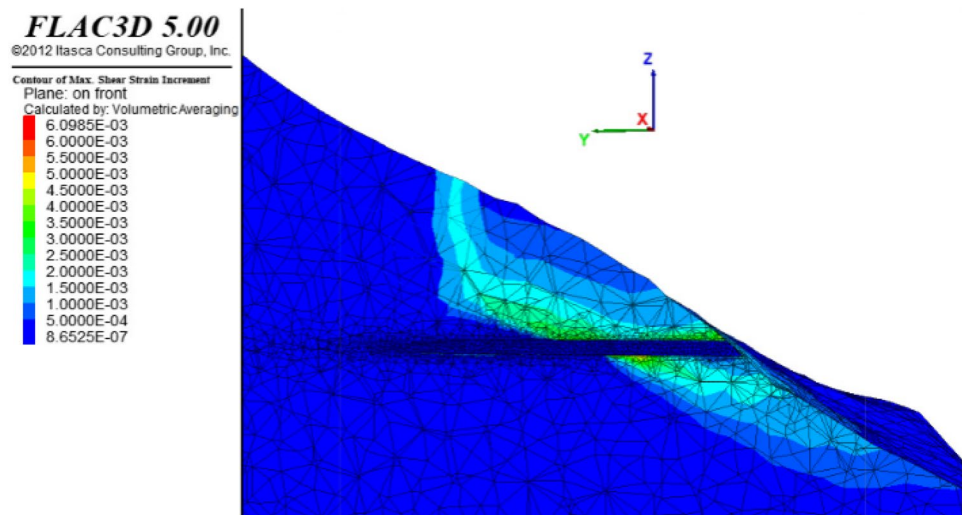

b) Displacement cloud diagram of slope in Y direction after excavation

c) Displacement cloud diagram of slope in Z direction after excavation

Fig. 13 Sectional cloud diagram of maximum shear strain increment of slope under rainfall condition after excavation

with cracks discovered on tunnel lining within 40 m of the tunnel portal. Third, as for Y-direction displacement of tunnel excavation simulation, the maximum displacement is at the location of 90 m above the tunnel on the slope surface, reaching 2.22 cm which is aligned with the ground surface displacement monitoring results in the y direction. Fourth, the maximum settlement acquired from tunnel excavation simulation of the Z-direction displacement is 8.73 cm, occurring at 160 m above the tunnel portal, which is also consistent with the crack observed onsite. Therefore, it turns out that the numerical model is validated by proving that numerical model results are compatible with corresponding in situ monitoring results and field investigation results.

Additionally, the interaction mechanism of the "landslide traction segment-tunnel longitudinal tensile failure" mode will be thoroughly discussed in this section from the perspective of time distribution and spatial distribution. In terms of time distribution, the spread of cracks at the rear edge of the landslide was first discovered on the slope's surface in December 2015, indicating that the slope was already in an unstable state before the tunnel excavation. In March 2016, the displacement monitoring points placed on the ground surface reflected that the ground surface was constantly creeping and deforming. With the excavation of the tunnel, diagonal tensile cracks spreading in the tunnel were discovered in March 2017. Under continuous construction disturbance, the cracks in the tunnel gradually expanded, accompanied by creep deformation of the landslide body. In the rainy seasons of 2018 and 2019, ground deformation occurred at the rear edge of the landslide. Therefore, the deformation of the landslide body occurred earlier than the deformation of the tunnel, and the time of continuous deformation of the landslide body occurred during the excavation of the tunnel, indicating that the deformation of the landslide body

was affected by the excavation of the tunnel. With the cracking deformation of the tunnel, the surface deformation of the landslide is intensified. Thus, the deformations of tunnel and landslide are mutually affected in terms of time distribution.

In terms of spatial distribution, the deformation area of the tunnel was exactly the position where the landslide traversed through, and the deformation range of the landslide and the deformation distribution range of the tunnel had good consistency in space. The cracks at the trailing edge of the landslide continued to enlarge, inducing the corresponding position of the tunnel to generate diagonal tensile cracks. With the penetration of the sliding surface, the landslide body gradually deformed, which also caused the tunnel to generate shear deformation. As the deformation of the tunnel continued to enhance, the landslide body also continued to deform. Therefore, the deformations of tunnel and landslide are mutually affected in terms of spatial distribution.

Suggested landslide prevention measures

The deformation of the tunnel and the deformation of the landslide are interrelated and affected each other. In order to effectively prevent the deformation of the landslide and the tunnel, the following four control principles are proposed, namely, stabilizing the landslide slope, limiting the deformation of the tunnel, controlling the local stress of the tunnel, and restraining the groundwater to soften slip surface. It is often considered to use strong support engineering structure, like anti-sliding piles, to reinforce the slope to solve the landslide deformation problems. However, this control measure only considers the stability of the landslide and neglect the problem of tunnel deformation. Since tunnels
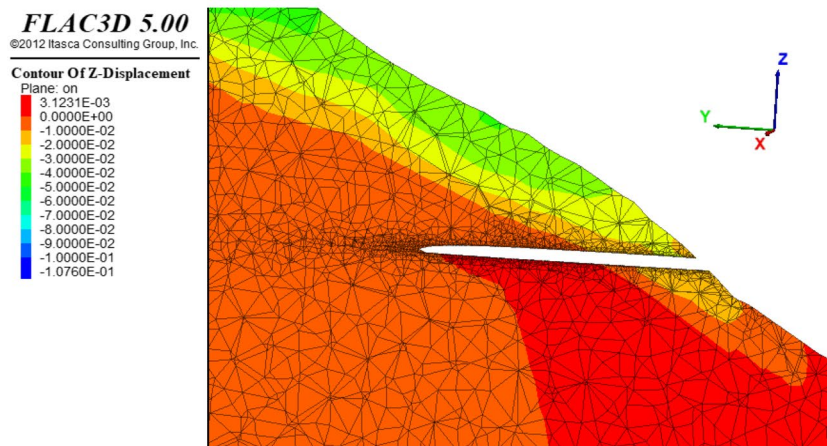
Fig. 14 Displacement cloud diagram of slope in the X, Y, and Z directions under rainfall condition after excavation
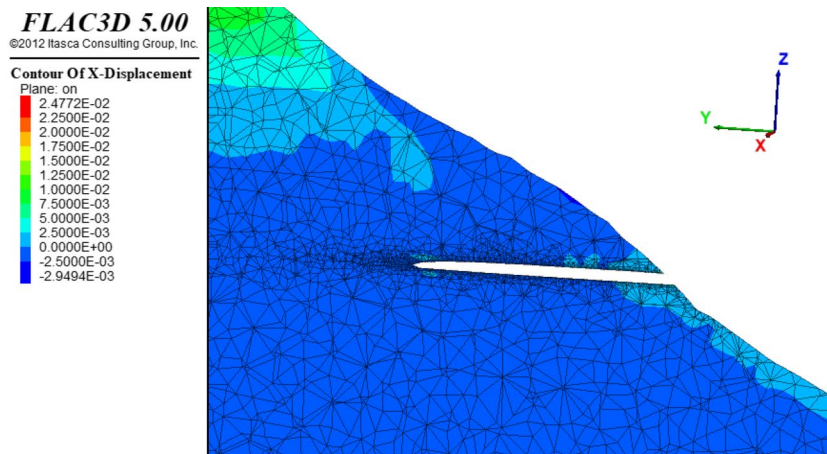
a) Displacement cloud diagram of slope in X direction under rainfall condition after excavation
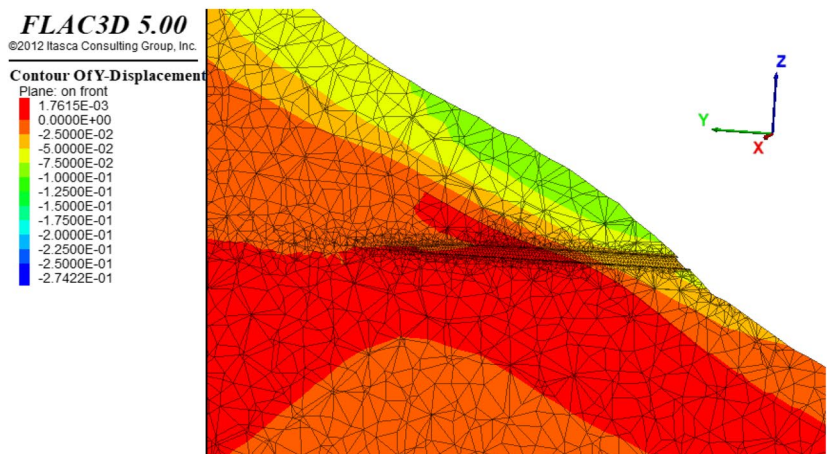
b) Displacement cloud diagram of slope in Y direction under rainfall condition after excavation

c) Displacement cloud diagram of slope in Z direction under rainfall condition after excavation

can only withstand small deformations, this control measure will still subject large landslide thrusts to tunnels. In order to limit the local deformation and stress, avoid the tunnel bearing and transferring the thrust of the landslide, and at the same time achieve the purpose of suppressing the

groundwater to soften landslide slip surface, a comprehensive landslide-tunnel deformation control measures based on the control grouting technology of the steel floral tubes is adopted, which has a series of advantages. First, the grout can fill the cracks and cavities in the rock body and also

form a support frame to bear the landslide thrust so that the porosity of the rock is reduced. Second, the filling of the grouting can also prevent the groundwater supplying to landslide slip surface, improving the strength and impermeability of the rock mass around the tunnel. Third, the steel floral tube of splitting grouting is used as a micro pile body. After extending into the stable bedrock, the grouting body is used to make the combination of the grouting pipe and the rock layer into a whole structure, reaching the effect of underground pile group. The effect of such underground pile group is equivalent to construct the tunnel in a relatively stable rigid body. This rigid body structure can not only meet the requirements of controlling the deformation of the tunnel, but also meet the role of transmitting and bearing the thrust of the landslide to a certain extent, reducing the thrust transmitted to the tunnel. Fourth, the technology can effectively solve the problems of low construction safety and long construction period. It has the characteristics of rapid construction, efficient treatment of landslides and tunnel deformation, and achieves the dual role of treating landslide hazard and improving tunnel stability.

Conclusions

By adopting field monitoring methods and using numerical simulation software to simulate the situation that the tunnel traverses the landslide in parallel and considering the three working conditions of natural condition, excavation condition, and rainfall condition, the stability and displacement of the slope and the tunnel, as well as the interaction mechanism of the "landslide traction segment-tunnel longitudinal tensile failure" mode have been proposed. The following conclusions are proposed:

(1) The "landslide traction segment-tunnel longitudinal tensile failure" mode is proposed. Tensile failure or shear dislocation failure tend to occur during the different stages of the interaction between the tunnel and the landslide. The landslide and the tunnel deformations are consistent in time and spatial distributions.

(2) Field monitoring results indicated that two sliding layers were discovered in the landslide, the shallow creep sliding layer and the deep creep sliding layer, which corresponded to the tensile failure and shear dislocation failure modes proposed in the "landslide traction segment-tunnel longitudinal tensile failure" mode, respectively.

(3) Numerical simulation results illustrated that under the natural condition the slope was generally in an unstable state. Under the influence of tunnel excavation disturbance, the initial stress equilibrium in the slope was disrupted, and the stress of the slope was redistributed. Under the rain-

fall condition, the rainwater increased the weight of slope and softened the deformation zone, which intensified the deformation of the landslide and the tunnel.

(4) Four control principles are proposed to counter with landslide-tunnel deformation problems, which are stabilizing the landslide slope, limiting the deformation of the tunnel, controlling the local stress of the tunnel, and restraining the groundwater to soften slip surface. The corresponding control measures based on the control grouting technology of the steel floral tubes are suggested.

Declarations

References

Alonso EE, Zervos A, Pinyol NM (2016) Thermo-poro-mechanical analysis of landslides: from creeping behaviour to catastrophic failure. Géotechnique 66(3):202–219. https://doi.org/10.1680/jgeot.15.LM.006

Avanzi GA, Galanti Y, Giannecchini R, Presti DL, Puccinelli A (2013) Estimation of soil properties of shallow landslide source areas by dynamic penetration tests: first outcomes from Northern Tuscany (Italy). Bull Eng Geol Environ 72(3):609–624. https://doi.org/10.1007/s10064-013-0535-y

Bandini A, Berry P, Boldini D (2015) Tunnelling-induced landslides: the Val di Sambro tunnel case study. Eng Geol 196:71–87. https://doi.org/10.1016/j.enggeo.2015.07.001

Barla G, Debernardi D, Perino A (2015) Lessons learned from deep-seated landslides activated by tunnel excavation. Geomech Tunn 8(5):394–401. https://doi.org/10.1002/geot.201500028

Barla G, Tamburini A, Del Conte S, Giannico C (2016) InSAR monitoring of tunnel induced ground movements. Geomech Tunn 9(1):15–22. https://doi.org/10.1002/geot.201500052

Bayer B, Simoni A, Schmidt D, Bertello L (2017) Using advanced InSAR techniques to monitor landslide deformations induced by tunneling in the Northern Apennines, Italy. Eng Geol 226:20–32. https://doi.org/10.1016/j.enggeo.2017.03.026

Chen HX, Zhang LM, Gao L, Zhu H, Zhang S (2015) Presenting regional shallow landslide movement on three-dimensional digital terrain. Eng Geol 195:122–134. https://doi.org/10.1016/j.enggeo.2015.05.027

Chen IH, Lin YS, Su MB (2020a) Computer vision-based sensors for the tilt monitoring of an underground structure in a landslide area. Landslides 17(4):1009–1017. https://doi.org/10.1007/s10346-019-01329-x

Chen Z, He C, Yang W, Guo W, Li Z, Xu G (2020b) Impacts of geological conditions on instability causes and mechanical behavior of large-scale tunnels: a case study from the Sichuan–Tibet highway, China. Bull Eng Geol Environ 79(7):3667–3688. https://doi.org/10.1007/s10064-020-01796-w

Das S, Mallik J, Deb T, Das D (2020) Quantification of principal horizontal stresses inside a tunnel: an application of Fracture induced Electromagnetic Radiation (FEMR) technique in the Darjeeling-Sikkim Himalayas. Eng Geol 279:105882. https://doi.org/10.1016/j.enggeo.2020.105882

Desrues M, Lacroix P, Brenguier O (2019) Satellite pre-failure detection and in situ monitoring of the landslide of the tunnel du Chambon, French Alps. Geosciences 9(7):313. https://doi.org/10.3390/geosciences9070313

Duan X, Hou TS, Jiang XD (2021) Study on stability of exit slope of Chenjiapo tunnel under extreme rainstorm conditions. Nat Hazards 107(2):1387–1411. https://doi.org/10.1007/s11069-021-04636-6

Fiorucci M, Iannucci R, Lenti L, Martino S, Paciello A, Prestininzi A, Rivellino S (2017) Nanoseismic monitoring of gravity-induced slope instabilities for the risk management of an aqueduct infrastructure in Central Apennines (Italy). Nat Hazards 86(2):345–362. https://doi.org/10.1007/s11069-016-2516-5

Gattinoni P, Consonni M, Francani V, Leonelli G, Lorenzo C (2019) Tunnelling in landslide areas connected to deep seated gravitational deformations: an example in Central Alps (northern Italy). Tunn Undergr Space Technol 93:103100. https://doi.org/10.1016/j.tust.2019.103100

Guo Z, Shi Y, Huang F, Fan X, Huang J (2021) Landslide susceptibility zonation method based on C5. 0 decision tree and K-means cluster algorithms to improve the efficiency of risk management. Geosci Front 12:101249. https://doi.org/10.1016/j.gsf.2021.101249

Holzleitner W, Kraft-Fish M, Imre B, Preuth T (2013) Austrian tunnelling expertise connecting the Kashmir valley to India/Österreichische Tunnelbaukompetenz verbindet das Kaschmirtal mit Indien. Geomech Tunn 6(1):13–24. https://doi.org/10.1002/geot.201300003

Huang F, Huang J, Jiang S, Zhou C (2017) Landslide displacement prediction based on multivariate chaotic model and extreme learning machine. Eng Geol 218:173–186. https://doi.org/10.1016/j.enggeo.2017.01.016

Huang L, Li J, Hao H, Li X (2018) Micro-seismic event detection and location in underground mines by using Convolutional Neural Networks (CNN) and deep learning. Tunn Undergr Space Technol 81:265–276. https://doi.org/10.1016/j.tust.2018.07.006

Iverson RM, George DL (2016) Modelling landslide liquefaction, mobility bifurcation and the dynamics of the 2014 Oso disaster. Géotechnique 66(3):175–187. https://doi.org/10.1680/jgeot.15.LM.004

Jiao YY, Wang ZH, Wang XZ, Adoko AC, Yang ZX (2013) Stability assessment of an ancient landslide crossed by two coal mine tunnels. Eng Geol 159:36–44. https://doi.org/10.1016/j.enggeo.2013.03.021

Kaya A, Akgün A, Karaman K, Bulut F (2016) Understanding the mechanism of slope failure on a nearby highway tunnel route by different slope stability analysis methods: a case from NE Turkey. Bull Eng Geol Environ 75(3):945–958. https://doi.org/10.1007/s10064-015-0770-5

Kaya A, Karaman K, Bulut F (2017) Geotechnical investigations and remediation design for failure of tunnel portal section: a case study in northern Turkey. J Mt Sci 14(6):1140–1160. https://doi.org/10.1007/s11629-016-4267-x

Komu MP, Guney U, Kilickaya TE, Gokceoglu C (2020) Using 3D numerical analysis for the assessment of tunnel–landslide relationship: Bahce–Nurdag Tunnel (South of Turkey). Geotech Geol Eng 38(2):1237–1254. https://doi.org/10.1007/s10706-019-01084-9

Konagai K, Numada M, Zafeirakos A, Johansson J, Sadr A, Katagiri T (2005) An example of landslide-inflicted damage to tunnel in the 2004 Mid-Niigata prefecture earthquake. Landslides 2(2):159–163. https://doi.org/10.1007/s10346-005-0057-1

Kromer RA, Abellán A, Hutchinson DJ, Lato M, Chanut MA, Dubois L, Jaboyedoff M (2017) Automated terrestrial laser scanning with near-real-time change detection–monitoring of the Séchilienne landslide. Earth Surf Dyn 5(2):293–310. https://doi.org/10.5194/esurf-5-293-2017

Lalagüe A, Lebens MA, Hoff I, Grøv E (2016) Detection of rockfall on a tunnel concrete lining with ground-penetrating radar (GPR). Rock Mech Rock Eng 49(7):2811–2823. https://doi.org/10.1007/s00603-016-0943-y

Lari S, Frattini P, Crosta GB (2014) A probabilistic approach for landslide hazard analysis. Eng Geol 182:3–14. https://doi.org/10.1016/j.enggeo.2014.07.015

Li Z, Huang H, Xue Y (2014) Cut-slope versus shallow tunnel: risk-based decision making framework for alternative selection. Eng Geol 176:11–23. https://doi.org/10.1016/j.enggeo.2014.04.001

Li C, Wu J, Tang H, Wang J, Chen F, Liang D (2015) A novel optimal plane arrangement of stabilizing piles based on soil arching effect and stability limit for 3D colluvial landslides. Eng Geol 195:236–247. https://doi.org/10.1016/j.enggeo.2015.06.018

Li W, Fan X, Huang F, Chen W, Hong H, Huang J, Guo Z (2020) Uncertainties analysis of collapse susceptibility prediction based on remote sensing and GIS: influences of different data-based models and connections between collapses and environmental factors. Remote Sens 12(24):4134. https://doi.org/10.3390/rs12244134

Lu N, Wayllace A, Oh S (2013) Infiltration-induced seasonally reactivated instability of a highway embankment near the Eisenhower Tunnel, Colorado, USA. Eng Geol 162:22–32. https://doi.org/10.1016/j.enggeo.2013.05.002

Lu L, Liang S, Luo S, Li J, Zhang B, Hu H (2018) Optimization of the construction technology of shallow-buried tunnel entrance constructed in residual slope accumulation of gravelly soil. Geotech Geol Eng 36(4):2391–2401. https://doi.org/10.1007/s10706-018-0470-6

Mandal S, Mondal S (2019) Statistical approaches for landslide susceptibility assessment and prediction. Springer International Publishing, Cham

Poisel R, Am Tinkhof KM, Preh A (2016) Landslide caused damages in a gallery. Rock Mech Rock Eng 49(6):2301–2315. https://doi.org/10.1007/s00603-015-0765-3

Pudasaini SP, Miller SA (2013) The hypermobility of huge landslides and avalanches. Eng Geol 157:124–132. https://doi.org/10.1016/j.enggeo.2013.01.012

Sun HY, Wong LNY, Shang YQ, Shen YJ, Lü Q (2010) Evaluation of drainage tunnel effectiveness in landslide control. Landslides 7(4):445–454. https://doi.org/10.1007/s10346-010-0210-3

Sun S, Li S, Li L, Shi S, Wang J, Hu J, Hu C (2019) Slope stability analysis and protection measures in bridge and tunnel engineering: a practical case study from Southwestern China. Bull Eng Geol Environ 78(5):3305–3321. https://doi.org/10.1007/s10064-018-1362-y

Tang H, Li C, Hu X, Wang L, Criss R, Su A et al (2015) Deformation response of the Huangtupo landslide to rainfall and the changing levels of the Three Gorges Reservoir. Bull Eng Geol Environ 74(3):933–942. https://doi.org/10.1007/s10064-014-0671-z

Tian X, Song Z, Zhang Y (2021) Monitoring and reinforcement of landslide induced by tunnel excavation: a case study from Xiamaixi tunnel. Tunn Undergr Space Technol 110:103796. https://doi.org/10.1016/j.tust.2020.103796

Tsao MC, Lo W, Chen WL, Wang TT (2021) Landslide-related maintenance issues around mountain road in Dasha River section of Central Cross Island Highway, Taiwan. Bull Eng Geol Environ 80(2):813–834. https://doi.org/10.1007/s10064-020-01967-9

Vassallo R, Mishra M, Santarsiero G, Masi A (2019) Modeling of landslide–tunnel interaction: the Varco d'Izzo case study. Geotech Geol Eng 37(6):5507–5531. https://doi.org/10.1007/s10706-019-01020-x

Walton G, Delaloye D, Diederichs MS (2014) Development of an elliptical fitting algorithm to improve change detection capabilities with applications for deformation monitoring in circular tunnels and shafts. Tunn Undergr Space Technol 43:336–349. https://doi.org/10.1016/j.tust.2014.05.014

Wang ZF, Shi FG, Li DD, Li H (2020) Tunneling-induced deep-seated landslides: a case study in Gulin County, Sichuan, China. Arab J Geosci 13(19):1–11. https://doi.org/10.1007/s12517-020-06048-5

Wei ZL, Shang YQ, Sun HY, Wang DF (2019) The effectiveness of a drainage tunnel in increasing the rainfall threshold of a deep-seated landslide. Landslides 16(9):1731–1744. https://doi.org/10.1007/s10346-019-01241-4

Wei ZL, Wang DF, Xu HD, Sun HY (2020) Clarifying the effectiveness of drainage tunnels in landslide controls based on high-frequency in-site monitoring. Bull Eng Geol Environ 79(7):3289–3305. https://doi.org/10.1007/s10064-020-01769-z

Wilfing L, Michael J, Schütz D (2021) Risk assessment of route options for the Hanau–Würzburg/Fulda railway project: Optimiertes Erkundungskonzept und Anwendung von BIM in frühen Projektphasen. Geomech Tunn 14(1):78–88. https://doi.org/10.1002/geot.202000036

Wu YM, Lan HX, Gao X, Li LP, Yang ZH (2015) A simplified physically based coupled rainfall threshold model for triggering landslides. Eng Geol 195:63–69. https://doi.org/10.1016/j.enggeo.2015.05.022

Yan L, Xu W, Wang H, Wang R, Meng Q, Yu J, Xie WC (2019) Drainage controls on the Donglingxing landslide (China) induced by rainfall and fluctuation in reservoir water levels. Landslides 16(8):1583–1593. https://doi.org/10.1007/s10346-019-01202-x

Zhang Y (2009) Evaluation of slope diseases and treatment projects[M]. Science Press, Beijing

Zhang H, Liu SG, Wang W, Zheng L, Zhang YB, Wu YQ et al (2018) A new DDA model for kinematic analyses of rockslides on complex 3-D terrain. Bull Eng Geol Environ 77(2):555–571. https://doi.org/10.1007/s10064-016-0971-6

Zhang Z, Zhang M, Zhao Q, Fang L, Ma S, Lv X (2021) A simplified analytical solution for deformation behavior of existing tunnels subjected to influences of landslides. Bull Eng Geol Environ 80(6):4651–4672. https://doi.org/10.1007/s10064-021-02230-5

Zhou X, Chen Z, Yu S, Wang L, Deng G, Sha P, Li S (2015) Risk analysis and emergency actions for Hongshiyan barrier lake. Nat Hazards 79(3):1933–1959. https://doi.org/10.1007/s11069-015-1940-2

Zhou H, Wang Y, Shen T, Feng Q (2019) The comprehensive treatment of the ancient landslide deformable body in the giant deep rock bedding based on the FLAC analysis model. Earth Sci Res J 23(4):303–308. https://doi.org/10.15446/esrj.v23n4.84008

Zhu C, Zhang J, Liu Y, Ma D, Li M, Xiang B (2020) Comparison of GA-BP and PSO-BP neural network models with initial BP model for rainfall-induced landslides risk assessment in regional scale: a case study in Sichuan, China. Nat Hazards 100(1):173–204. https://doi.org/10.1007/s11069-019-03806-x